Food Hydrocolloids 171 (2026) 111854

Contents lists available at ScienceDirect

Food Hydrocolloids

journal homepage: www.elsevier.com/locate/foodhyd

Deposition of hierarchically porous cellulose microfibril films *via* emulsion templating and drying at ambient temperature

Hyung-Ju Kim [a,b], Yan Zeng [a], Krassimir P. Velikov [c,d,e,*], Orlin D. Velev [a,**]

[a] Department of Chemical & Biomolecular Engineering, North Carolina State University, 911 Partners Way, Raleigh, NC, 27695-7905, USA
[b] Nuclear Facility Cleanup Technology Division, Korea Atomic Energy Research Institute, 989-111 Daedeok-daero, Yuseong-gu, Daejeon, 34057, South Korea
[c] Unilever Innovation Centre Wageningen, Bronland 14, 6708 WH, Wageningen, the Netherlands
[d] Institute of Physics, University of Amsterdam, Science Park 904, 1098 XH, Amsterdam, the Netherlands
[e] Soft Condensed Matter, Debye Institute for Nanomaterials, Utrecht University, Princetonplein 1, 3584 CC, Utrecht, the Netherlands

ARTICLE INFO

Keywords:
Microfibrillated cellulose
Porous material
Emulsion
Hydrophobicity
Self-cleaning material

ABSTRACT

Porous films and coatings based on biocompatible natural renewable materials such as cellulose are of interest to diverse fields such as biomedical devices, insulation, separations, ion exchange, sensing, and packaging. We report the fabrication of hierarchically macro- and nanoporous films of microfibrillated cellulose (MFC) using a novel single-step method based on emulsion templating with recyclable volatile oils. The hierarchical (dual-level) porous cellulosic films are deposited at room temperature by drying of volatile oil-in-water emulsions stabilized by MFC and surfactants. A three-step formation mechanism, based on the evolution of the emulsion droplet size, is proposed. One key factor controlling the resultant structure of the porous films is the vapor pressure difference between the oil and water. Templating with droplets of oil with vapor pressure of the same order as, or lower than, that of water results in formation of macroscopic porous structures. Addition of surfactant can significantly increase the porosity and the thickness of the films by suppressing the coalescence/coarsening of the oil droplets and reducing the flattening effect caused by capillary forces. We demonstrate that these films can be functionalized by silylation to obtain hydrophobic hierarchical dual-level porous films with water contact angles of 70~116°.

1. Introduction

Porous organic and inorganic structures form the basis of commercial stable materials in diverse fields such as ion exchange (Bennett et al., 2000; Nouar et al., 2009), insulation (Baxter et al., 2000), adsorption (Chaikittisilp et al., 2011, 2013), separation (Gelb et al., 1999; Jang et al., 2011; Kim et al., 2013, 2014, 2015; J. R. Li et al., 2009; Minakuchi et al., 1996; Seo et al., 2000), sensing (Beauvais et al., 2000; W. Y. Li et al., 2005; C. Wu et al., 2006), catalysis (Mehnert et al., 1998; Proust et al., 2008), and tissue engineering (Hollister, 2005). In the past decades, emulsions and foams stabilized by inorganic particles including silica (Binks & Horozov, 2005; Dickinson et al., 2004), alumina (Juettner et al., 2007; Kishimoto et al., 2007), zirconia (Higashiwada et al., 2007; Sherif & Shyu, 1991), and metal organic framework (Han et al., 2024; T. Wu et al., 2023) have been used as precursors for such materials. These porous materials are often brittle, inflexible, non-biodegradable and sometimes not biocompatible. In addition, the common conventional freeze-drying method used to fabricate those porous materials, is energy consuming, expensive and difficult to control. Earlier, macroporous polymers or polymer foams have been fabricated from emulsion (Krajnc et al., 2005; Tokuyama & Kanehara, 2007) or foamed emulsion templates (Imhof & Pine, 1997; Yuan & Su, 2006). However, these studies involve complicated processes such as UV polymerization and energy intensive processing steps (such as freeze drying or vacuum drying). Therefore, the development of simple low-cost methods that can create biocompatible and biodegradable materials with tunnelable porosity, preferably from renewable sources, is still a challenge.

This article is part of a special issue entitled: 19th Food Colloids Conference published in Food Hydrocolloids.

* Corresponding author. Unilever Innovation Centre Wageningen, Bronland 14, 6708 WH, Wageningen, the Netherlands.
** Corresponding author. Department of Chemical & Biomolecular Engineering, North Carolina State University, 911 Partners Way, Raleigh, NC, 27695-7905, USA.
E-mail addresses: krassimir.velikov@unilever.com (K.P. Velikov), odvelev@ncsu.edu (O.D. Velev).

https://doi.org/10.1016/j.foodhyd.2025.111854
Received 1 December 2024; Received in revised form 2 August 2025; Accepted 8 August 2025
Available online 14 August 2025

The sustainable fabrication of advanced materials by using ubiquitous natural resources is a growing field, which draws significant attention by researchers in both basic and applied sciences (Hamer & Al-Awadhi, 2000; Ahmad et al., 2025). The most abundant bioresource in nature is cellulose, which in the form of microfibrillated cellulose (MFC) serves as matrix of many materials such as paper (Andresen et al., 2006; Aulin et al., 2010), food (Plackett et al., 2010), cosmetics (Siró & Plackett, 2010), pharmaceutics (Pandey, 2021) and nanocomposites (Sherbo et al., 2018). MFC is biodegradable, biocompatible, and sufficiently inert to environment. It is also valuable for material science perspective due to its extremely large specific surface area, high tensile strength, and elasticity. MFC aerogels have been widely explored (Ferreira et al., 2023; Sun et al., 2021), but because of the use of expensive drying processes, their application has been hindered. Such aerogels also have micropores that enable their application in cell tissue engineering; however, dual porosity is typically required, which is difficult to achieve (Lee et al., 2008; Murphy & O'Brien, 2010; Naseri et al., 2016; Pircher et al., 2015). The high tensile strength and elasticity contributed by the crystalline domains in MFC enable its broad applications as a rheology modifier being used, for instance, to promote the stability of emulsions (Lam et al., 2014).

We report results on how the drying of MFC-stabilized emulsions with droplets from volatile oils could be used to fabricate MFC porous films with various structures and thicknesses. The results of room-temperature drying of emulsions from oils with vapor pressure higher, or the same order as the one of the continuous water phase are compared and shown to have a critical structural effect. The mechanism of the hierarchically porous structure formation during evaporation is interpreted *via* the time evolution of the emulsion oil droplet size. By varying the oil volume fraction and the surface tension of the aqueous phase, we are able to tune the structure and/or the thickness of the resulting dry porous films. Further, porous films are functionalized using methyltrichlorosilane to tailor their hydrophobicity.

2. Experimental section

2.1. Materials

The MFC from wood (3 wt% in water dispersion) was obtained from MeadWestvaco (Richmond, VA). The following reagents from commercial suppliers were used as received without further purification: hexane (Purity 99+%, Fisher), octane (Purity 99+%, Fluka), decane (Purity 99+%, Sigma-Aldrich), polyoxyethylenesorbitan monolaurate (Tween 20, Sigma-Aldrich), sodium dodecyl sulphate (SDS, Purity 99+%, Sigma-Aldrich), and methyltrichlorosilane (Sigma-Aldrich). Deionized water from Millipore (18.2 MΩ cm) was used in all experiments.

2.2. Synthesis

MFC dispersion (pH 7, and total solid concentration 660 mg/L) was diluted with deionized water. The diluted MFC dispersion (0.3–3 wt%) was passed through a homogenizer (IKA® Magic LAB®, Germany) at 10 krpm for 10 min. An aliquot of 0.3 wt% MFC dispersion, *x* g, was added into a small glass vial and *(10-x)* g volatile solvent used as oil phase (i.e., hexane, octane, or decane) was added afterward to keep the total amount as constant at 10 g. Emulsion was prepared by shaking the sealed vial for 1 min at frequency around 1.5 Hz. The emulsion was then poured evenly over the bottom of a Petri dish (round, polystyrene, 60 mm D × 15 mm H, Fisher Scientific) and left to dry at ambient temperature and pressure. To investigate the effect of surface tension, 1 g of surfactant solution (0.16 wt% aqueous Tween 20 or 0.5 wt% aqueous SDS) was added into the precursor emulsion before pouring it into the Petri dish.

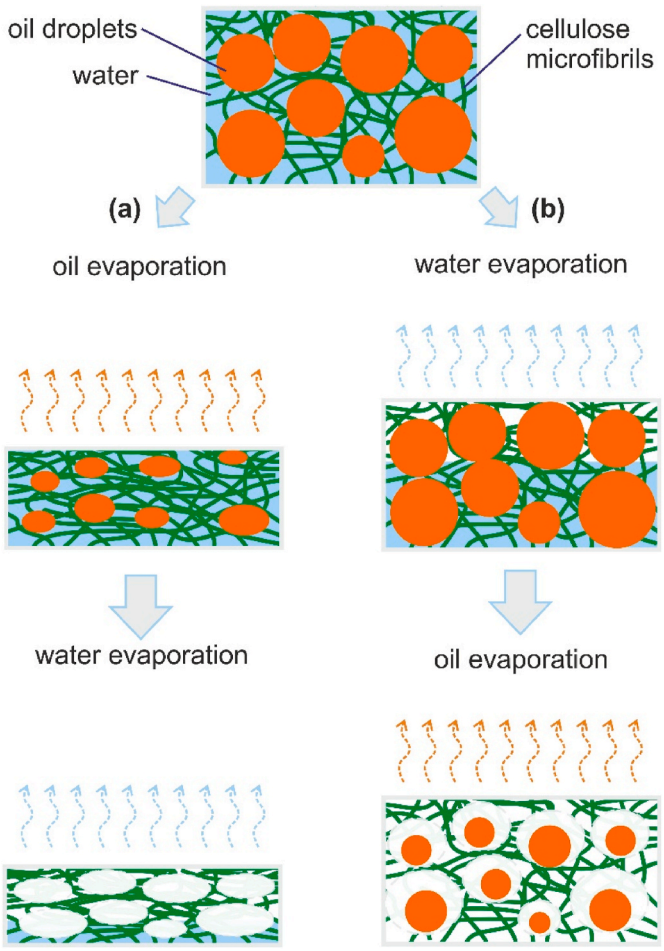

Scheme 1. A schematic illustration of the impact of varying evaporation rates between the disperse and continuous phases, at same initial volume fraction of the disperse phase, determined by the vapor pressure of the volatile oil. Two extreme scenarios of the drying process and the resultant mesostructures are depicted: (a) when oil evaporates considerably faster than water (e.g., hexane in this study), and (b) when water evaporates significantly faster than oil (e.g., decane in this study).

2.3. Silylation

Prepared porous films were silylated with methyltrichlorosilane. Prior to silylation, the porous films were evacuated in an oven at 70 °C overnight to remove physically adsorbed moisture. The evacuated porous film was placed inside of a PYREX® media bottle (100 mL, VWR) containing 100 μL of methyltrichlorosilane. The bottle was closed tightly and maintained at a 70 °C for 24 h of reaction time. Then, the porous films were dried at room temperature before measuring water contact angle (WCA).

2.4. Characterization

Micrographs of emulsions and dry films were recorded with a digital camera (Canon 5D). The optical microscope (Olympus BX61) with objective magnification in 10 × was used to observe the emulsion droplet during certain periods of time and the final pores of the dry film. The droplet size and pore size were determined by taken images. Scanning electron microscope (SEM, Joel 6400) was performed to examine both in-plane and lateral structure of dry films at high magnification. The SEM samples were coated with gold-palladium to prevent image distortion due to surface charge. Experimental data on the surface tension of water, Tween 20, and SDS at 20 °C were taken from elsewhere

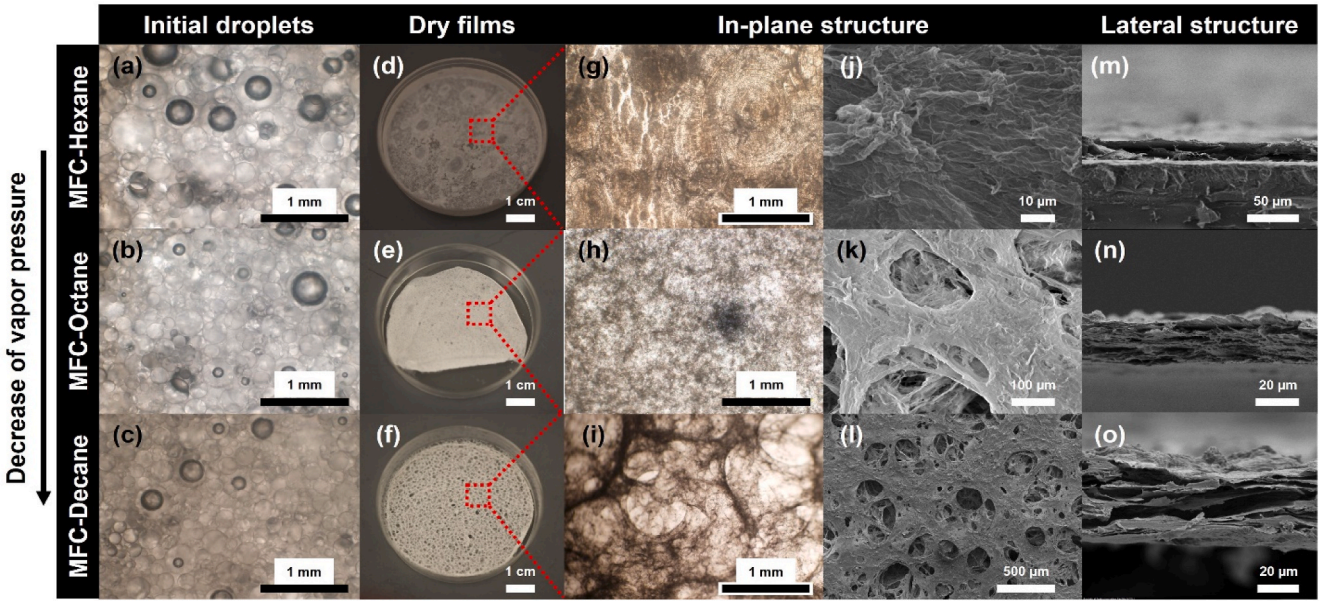

Fig. 1. Effect of oil type on film morphology on the macro and microscale: (a-c): optical microscopic images of emulsion droplets prepared by shaking 7.5 g of 0.3 wt % MFC dispersion and 2.5 g of hexane/octane/decane (i.e., 25 wt% of total pre-mixed solution). Darker spheres are air bubbles which disappear after certain time; (d-f): photographic images of dry films; (g-i): optical microscopic images of the in-plane porous structure of dry films; (j-l): SEM images of the in-plane porous structure of dry films; (m-o): SEM image of lateral structure of dry films.

(Mysels, 1986; Niño & Patino, 1998; Wege et al., 2008). Static WCA was measured on the different porous films using a telescopic goniometer (FTA 1000 Drop Shape Instrument). A drop of deionized water was dispensed onto the sample surfaces. Both the right and left angles between the sample surface and the tangent line to the droplet were measured.

3. Results and discussions

3.1. Vapor pressure of volatile oil

The morphology and porosity of the residual porous films depend on the rate of the evaporation of the droplets relative to water from the surrounding aqueous-MFC matrix. These differences will determine which phase, continuous (i.e., water) or disperse (i.e., oil) will evaporate faster and create voids in the MFC-gel. Thus, the type of oil-in-water emulsion used as a template in the MFC-gel has an important role. The presence of emulsion droplets in the MFC-gel reinforces the gel and prevents the rapid collapse of the film during the water evaoration. Simultaneously, water evaporation increases the concentration of MFC between oil droplets, enhancing the formation of a dense fibrillar network that sterically hinders coalescence. Although the reduced volume of the continuous phase brings droplets into closer proximity, the dominant effect appears to be the increased stabilizing capacity of the concentrated MFC, resulting in reduced coalescence during drying. This synergistic action between the oil droplets and the MFCs allow for both preserving the nanoscale pores in the MFC networks and the microscale pores created by the volatile oil droplets, hence, creating the template enabling the creation of films with dual porosity.

The interplay between the evaporation rates of water and the oil can be used to create and control the final mesoscale porous structure. Scheme 1 shows the expected structural evolution in two cases with very large difference in the evaporation rate of the dispersed oil phase and continuous aqueous phase. Three volatile oils were chosen as the templating phase of the MFC-gel emulsions (i.e., hexane, octane, and decane) based on their vapor pressure difference with water. The evaporation rate of the oils at constant surface area (i.e. similar averaged droplet sizes) can be assumed to be linearly dependent on the vapor pressure (Mackay & Van Wesenbeeck, 2014). The vapor pressure of hexane is 17.6 kPa at 20 °C (Stull, 1947). As it is much higher than water, the hexane droplets evaporate before the cellulosic fibril dispersions dry out. The rate of evaporation determines whether the water leaves the film first, leaving behind the cellulose structure around the droplets that are still intact with little ability for the fibril to re-arrange further, or whether the droplets evaporate before the MFC network is "locked" in place by water drying. The vapor pressure of octane is 1.47 kPa at 20 °C (Stull, 1947), which is of the same order as vapor pressure of water, 2.3 kPa at 20 °C (Wexler, 1976). In this case, octane evaporates at approximately the same rate as water. Thus, one would expect that the compression of the film will be closing the voids created from the evaporating droplets and that the final dry material contains fewer pores. On the contrary, the vapor pressure of decane is 195 Pa at 20 °C (Stull, 1947), thereby water evaporates much faster than decane in the MFC-decane emulsion system. Thus, more pores will be preserved after drying, sustained by the oil droplets that evaporate last. A schematic of the expected effect of vapor pressure on the drying process of MFC-volatile solvent-based emulsions is shown in Scheme 1, when oil evaporates much faster (e.g., hexane in this study shown in Scheme 1a), and when water evaporates much faster (e.g., decane in this study as shown in Scheme 1b).

The experimental results clearly demonstrate that the relative evaporation rate has a dramatic effect on the structure of the final cellulose films. Optical microscopic images of initial emulsion droplets, photographic images of final dry films, zoomed-in optical microscopic images of in-plane structure of dry films, and the in-plane as well as lateral SEM images of dry films, for the three different oil-water systems are presented in Fig. 1. The initial average droplet sizes of emulsions prepared with all three volatile oils are similar (Table S1 in Supporting Information); however, the in-plane structure of the deposited dry films is significantly different. As shown in the SEM images (Fig. 1j–o), we obtained a thin, porous film of 20 μm in thickness from drying MFC-octane emulsion with average pore size around 219 ± 60 μm, while the porous film from MFC-decane emulsion had larger average pore size around 477 ± 196 μm and slightly higher thickness of 30 μm (Table S1 in Supporting Information). No discernible large pores are observed in the dry film prepared from MFC-hexane emulsion, instead these films

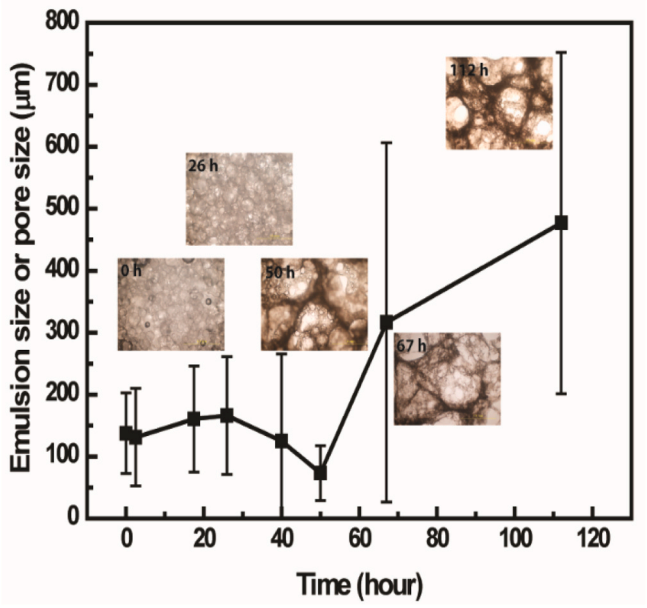

Fig. 2. Evolution of emulsion droplet size and pore size for MFC-decane gel prepared by 7.5 g of 0.3 wt% MFC dispersion and 2.5 g of decane: the droplet size of decane emulsion (i.e., 25 wt% of total pre-mixed solution) increases initially within the first 30 h, suggesting that droplets coalescence dominates during water and decane evaporation. A decrease in the average emulsion droplet size is then recorded between 30-50 h, indicating a phase separation of larger oil droplets. Finally, an increase in pore size occurs, reflecting a flattening effect due to the capillary force.

display characteristic ring patterns. Thus, volatile oil with vapor pressure of the same order or lower than that of water is selected in order to obtain porous films. In this way the oil droplets evaporate later that the water medium and are able to provide reinforcement of the MFC network and prevent it from collapse during the drying process. This correlates with the aforementioned discussion on the effect of difference between vapor pressure of volatile oil and water, which determines the difference in evaporation rate between the two phases.

3.2. Elucidation of the drying mechanism

The average size of the microscale pores observed in the final dry films is much larger than the initial emulsion droplet size. This is because of coalescence, disproportionation, and capillary force flattening the droplets during evaporation of water. As the water evaporates, the concentration of dispersed emulsion droplets increases, leading to closer proximity and potential coalescence. These phenomena contribute to changes in droplet size distribution during drying (Dekker et al., 2020). To understand more intricately the mechanisms occurring during room-temperature drying, we measured the droplet size of emulsions prepared with 0.3 wt% MFC dispersion and 25 wt% decane against time and plotted the results in Fig. 2 (further detailed optical microscopy images are shown in Fig. S1 of Supporting Information). The average emulsion droplet size remains constant or increases slightly in the initial 30 h and then decreases to a minimum after 50 h. After that, it increases again as film dries out, reaching a final state (value at ≈ 480 μm). The corresponding distributions of emulsion droplet size and pore size for MFC-decane gel are extracted by ImageJ software and shown in Fig. S2 of Supporting Information. The observed three-step drying process—initial droplet growth due to coalescence, size reduction from oiling-out, and final size increase from capillary flattening—is consistent with findings in complex suspension drying. These stages result in the evolution of droplet sizes and the eventual formation of pores in dried films (Yang et al., 2025). In the first step, the coalescence and/or

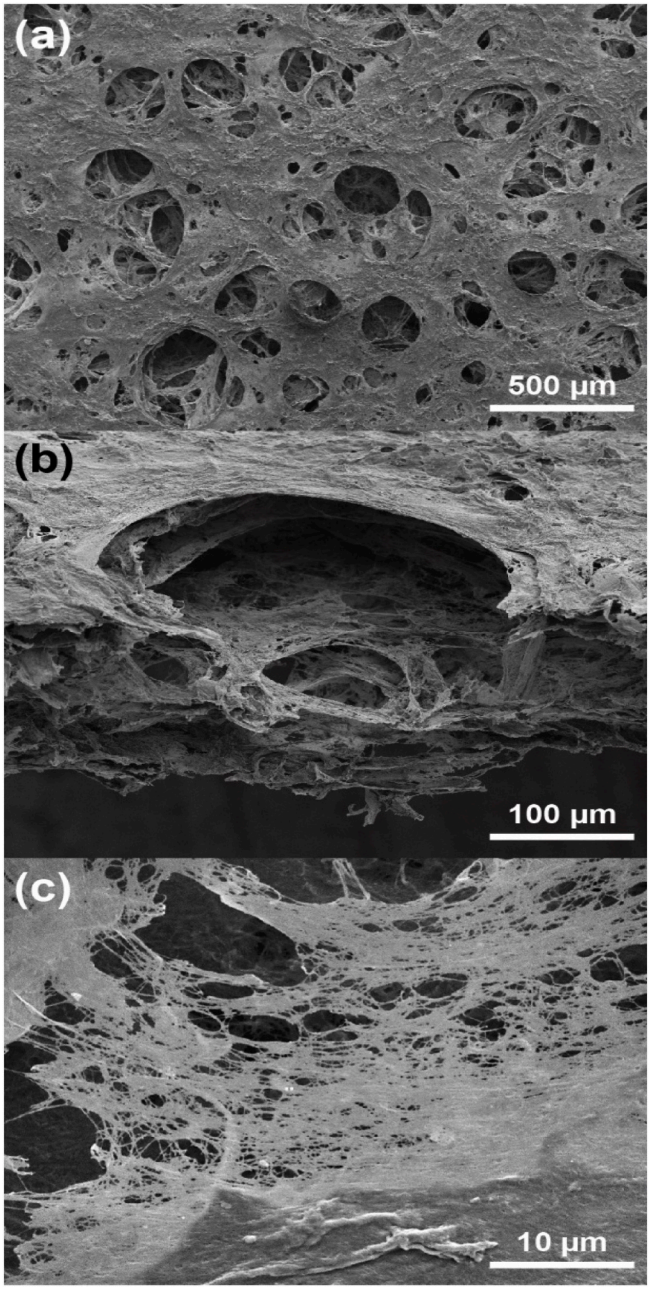

Fig. 3. SEM images of the (a) in-plane structure, (b) 60° titled structure of dry film, and (c) the zoomed-in individual cellulose microfibrils as the building blocks of dry film prepared from 7.5 g of 0.3 wt% MFC dispersion and 2.5 g of decane (i.e., 25 wt% of total pre-mixed solution).

coarsening dominate the growth of emulsion droplets. In the second "oiling-out" step, large droplets can break through the top of emulsion film and form a separated layer of oil phase (all droplets are expected to move upwards and larger droplets will experience larger buoyancy force). Since only smaller droplets remain trapped in the MFC-gel phase, the average droplet size decreases. In the meantime, the three-dimensional network of MFC around former bigger droplets is preserved although some of the bigger droplets escape to the top (i.e., cream). When the thin film dries further, the capillary forces arising during the evaporation of water induce the flattening of decane droplets which leads to a visible increase in the droplets diameter when optically examining the in-plane structure. At the end, the final evaporation of decane in the droplets leaves behind microscale pores in the final dry film. Thus, the final dry film is much thinner than the initial film before

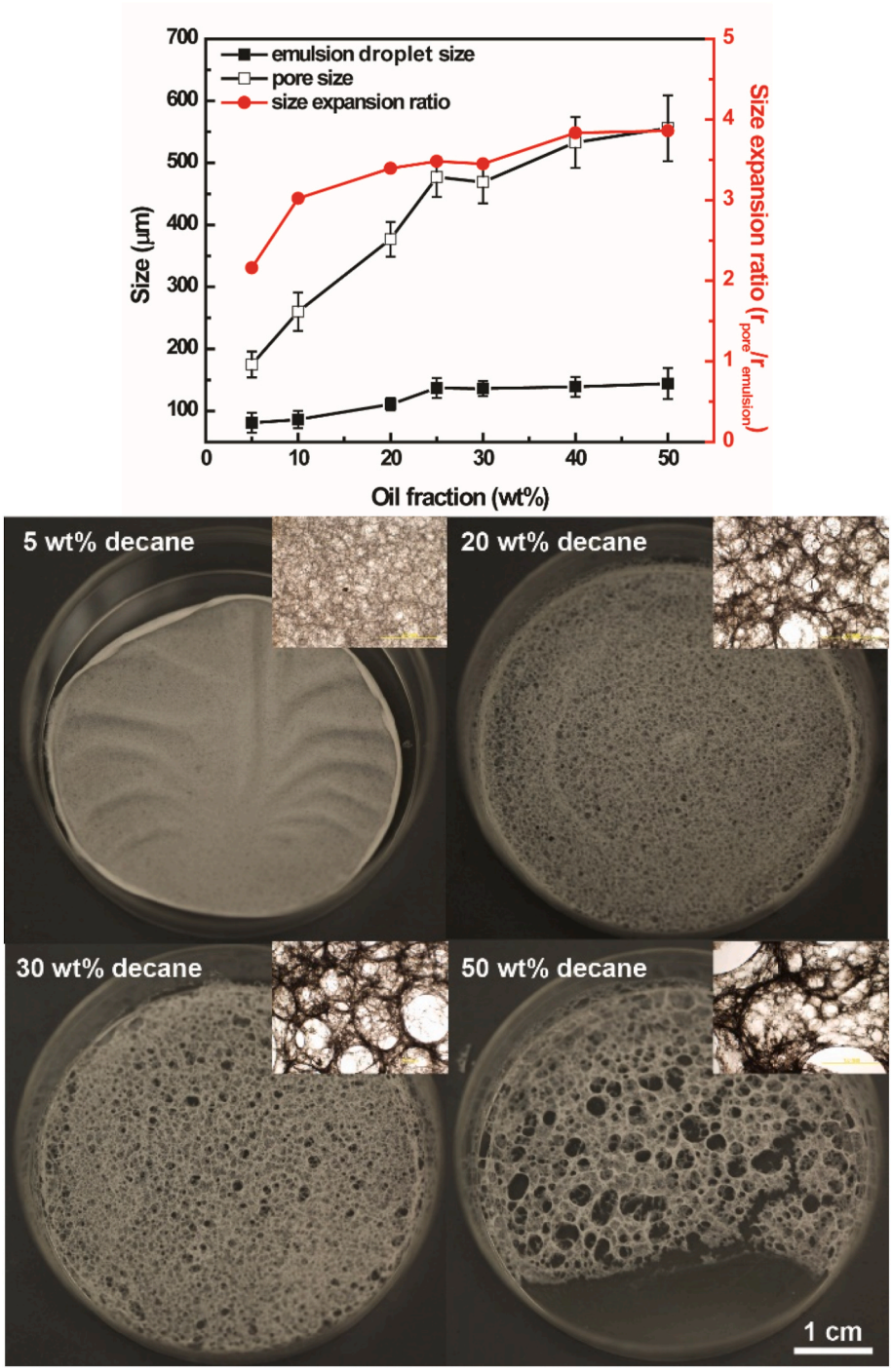

Fig. 4. (Top) The emulsion droplet size, pore size, and the corresponding size expansion ratios as a function of decane weight fraction ranging from 5 to 50 wt%; (Bottom) Photographic images of dry films with high magnification of the optic microscopic images prepared at a fixed initial MFC concentration (0.3 wt%) with varying decane volume fractions ranging from 5 to 50 wt%.

drying (i.e., 0.65 cm) due to capillary force induced flattening effect during solvent evaporation.

The SEM images in Fig. 3 present the structure of the dry porous films prepared from MFC-decane emulsion. The pores formed by the dry MFC have varying magnitude in size and are organized hierarchically (Mohan et al., 2017). The size varies from several hundred microns to a few microns contributed both from droplets coalescence/coarsening and capillary force induced flattening effect as mentioned above. More importantly, those pores are not only formed on the surface of the dry film (Fig. 3a), but also observed in each inner layer of the dry material (Fig. 3b) which is three-dimensionally interconnected by the cellulose microfibrils. Fig. 3c zooms down to the level of the matrix building blocks, i.e., the individual cellulose microfibrils, which have size around several nanometers in width and several tens of microns in length, as shown in Fig. S3 of Supporting Information. The MFC network is also porous with length scale below a micron. This hierarchical structure of the film consisting of micropores and a nanoscale network provides benefits in both tunable permeability and mechanical strength due to the fine MFC network.

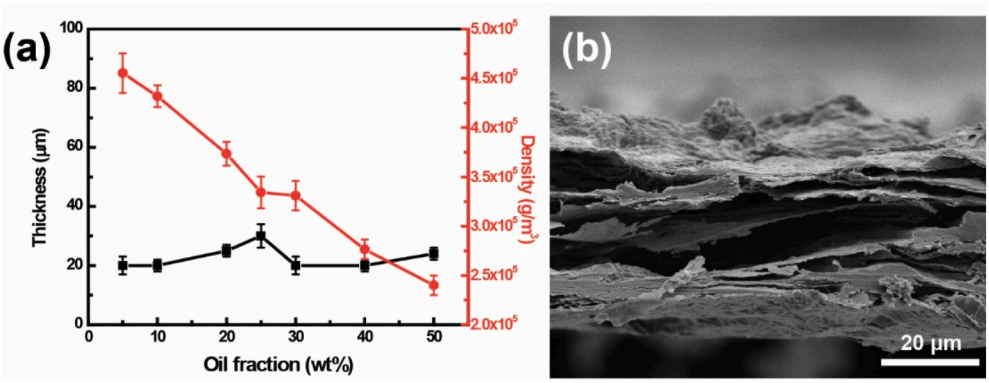

Fig. 5. (a) Thickness (black line) and density (red line) of the dry films, prepared at a fixed initial MFC concentration (0.3 wt%), as a function of decane weight fraction ranging from 5 to 50 wt%; (b) Lateral SEM image of the dry film emulsified from 0.3 wt% of MFC and 25 wt% of decane. (For interpretation of the references to colour in this figure legend, the reader is referred to the Web version of this article.)

3.3. Pore size control by adjusting oil fraction

The mechanism suggested above highlights several parameters controlling the pore size of the final dry film, including the initial emulsion droplet size, the coalescence and coarsening rate, and the capillary force. Because of the nature of the emulsification process, the varying of the oil volume fraction in the emulsions allows tuning the droplet size and then the pore size of final film as shown in Fig. 4. It was found that increasing the oil concentration led to larger droplet sizes and increased polydispersity, particularly at lower emulsifier concentrations

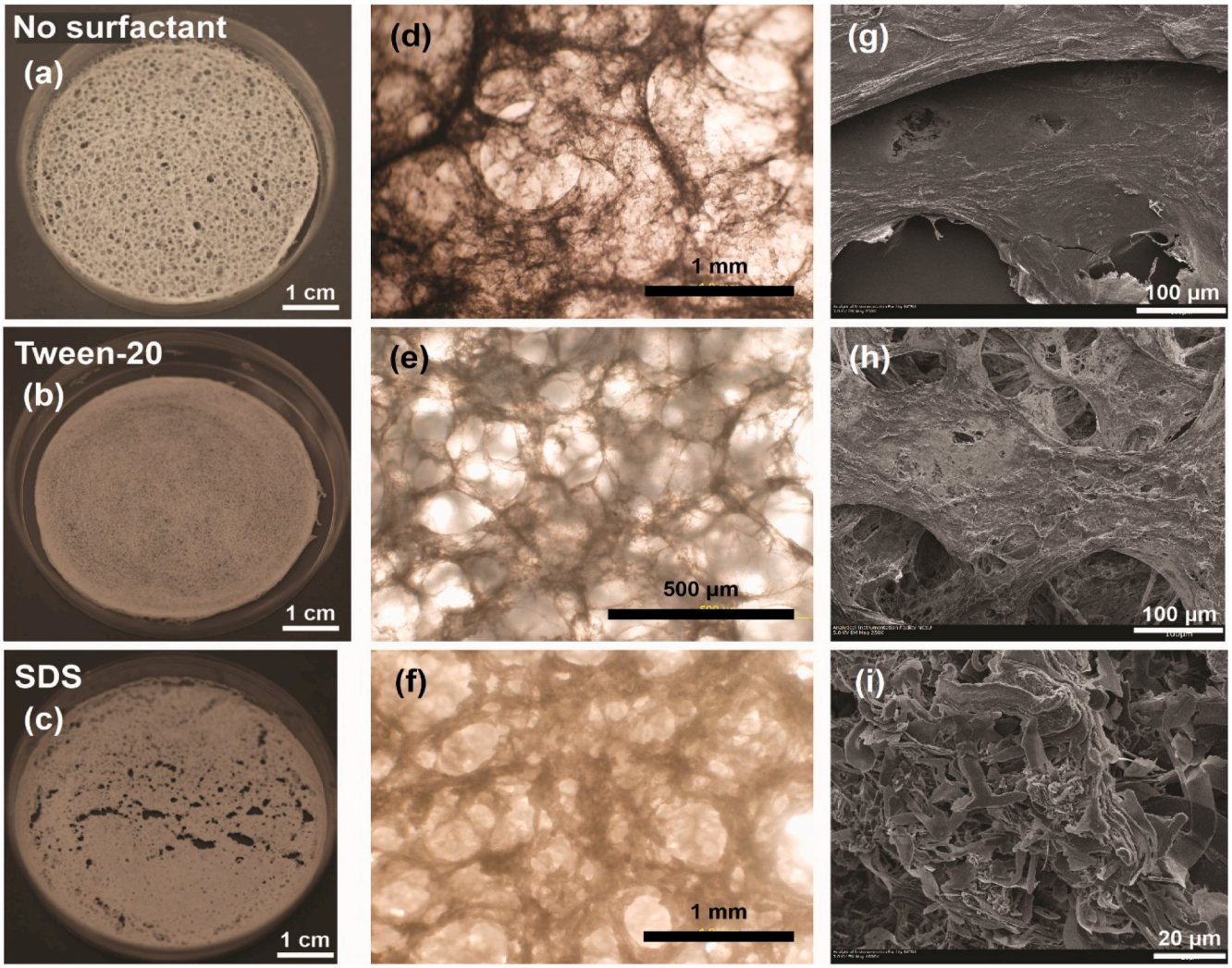

Fig. 6. (a-c): Photographic image of the dry film prepared from emulsion initially containing 0.3 wt% MFC (7.5 g), 25 wt% decane (2.5 g) without surfactant, with addition of 1 g of 0.16 wt% aqueous Tween 20 solution, and with addition of 1 g of 0.5 wt% aqueous SDS solution. (d-f): Optical microscopic images of the in-plane porous structure of dry films; (g-i) SEM images of the in-plane porous structure of dry films.

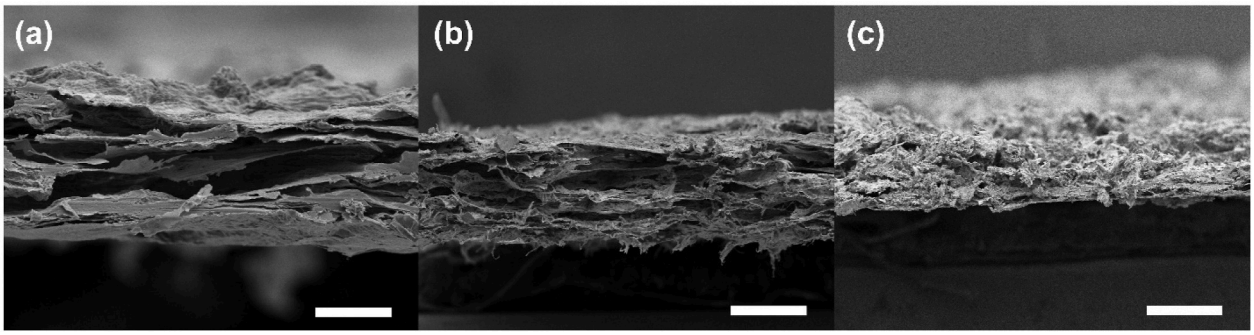

Fig. 7. Lateral SEM images of dry films prepared from emulsion initially containing 0.3 wt% MFC (7.5 g), 25 wt% decane (2.5 g) under conditions of (a) without surfactant, (b) with Tween 20, and (c) with SDS. Scale bar is 200 μm.

and shorter homogenization times (Dapčević Hadnađev et al., 2013). This is attributed to insufficient emulsifier to stabilize the increased oil-water interface, resulting in enhanced coalescence. The emulsion prepared with 50 wt% decane at a fixed initial MFC concentration (0.3 wt%) contains droplets 1.77 times larger in size than that of prepared with 5 wt% decane, while the corresponding pore size of dry film increases about 3.2 times (additional data are shown in Table S2 of Supporting Information). This indicates that the emulsion droplet size has a much less pronounced linear relationship with decane fraction, while the pore size of final film has linear relationship with decane fraction. This is because the initial emulsion droplet size remains almost the same regardless of the decane fraction, but the number of droplets increases with decane weight fraction. The slight droplet size increase in the range from 10 to 25 wt% is due to faster coalescence/coarsening by a larger number of emulsions. Different from emulsion droplet size, the pore size of final film is based on the result of completed coalescence/coarsening, thereby higher fraction of decane leads to larger final pore size of film. This can be quantified by the size expansion ratio, which is the ratio of the final pore size to the initial droplet size, $r_{pore}/r_{emulsion}$. This value indicates how the final pore size is developed from the initial size of the emulsion droplets. It increases from 2.5 to 4 as the oil volume fraction increases from 5 to 50 wt%. This result indicates the general relationship that small droplets at lower initial oil volume fraction yield many small pores. However, the slight increase of the expansion ratio as the initial oil fraction increases might be due to faster coalescence/coarsening rate at higher oil volume fraction which tailor the density and size of the big pores.

The thickness of dry films was determined by measuring the width of their lateral SEM images, and found to be independent of the oil fraction. The film thickness is consistently ≈20 μm for films prepared at varied oil fractions; thus the calculated film density decreases linearly with oil volume fraction as shown in Fig. 5. The dry film consists of around ten sub-layers and each layer is around several microns in thickness. This indicates that the flattening effect of the capillary force accompanied with water evaporation drives the three-dimensional network of cellulosic microfibrils around pores to pack densely and to form connected layers. These effects, occurring in the third step of the drying process are determining the final film thickness.

Because that the total amount of pre-mixed MFC suspension is always constant (10 g), the total concentration of MFCs in the final emulsion decreases as the oil volume fraction increases. One might expect that the thickness of the dry films deviates from each other and is proportional to the concentration of MFC in emulsions while the concentration in the aqueous phase remains constant. However, the small changes in the thickness of the final dry films at different oil volume fraction (also varied concentration of cellulosic fibrils) suggests that capillary forces play an important role in the degree of collapsing of the MFC-gel (at similar volume of the emulsion V_0 , the initial height of the solution in Petri dish with radius R is approximately the same: 0.65 cm). Another important parameter is the volume fraction φ_{oil} of the dispersed

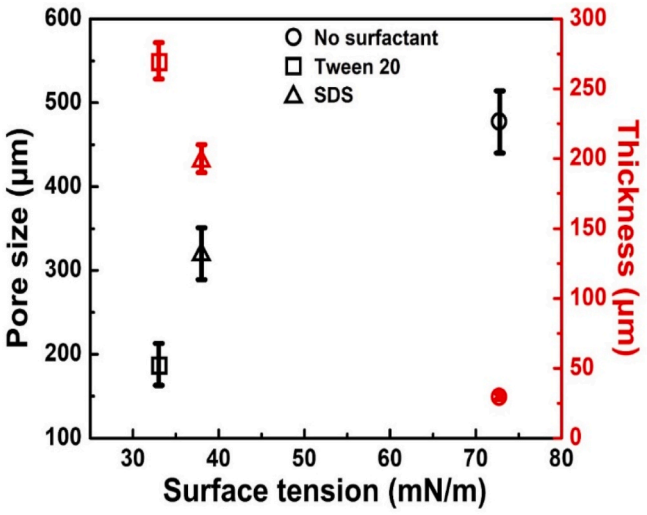

Fig. 8. Pore size (black symbol) and thickness (red symbol) of the dry films prepared from emulsion initially containing 0.3 wt% MFC (7.5 g), 25 wt% decane (2.5 g) in systems without surfactant (round) and with surfactant added (square for Tween 20 and triangle for SDS) as a function of surface tension of water-air interface. (For interpretation of the references to colour in this figure legend, the reader is referred to the Web version of this article.)

oil phase, which also contributes to the flow and elasticity of the drying film. Additionally, the increased porosity is expected to decrease the film elasticity (e.g., the porosity has an effect on elastic moduli of polymer foams) and make them more brittle (Drozdov & de Claville Christiansen, 2020). Thus, we find that in our system the capillary force compresses films to similar thickness regardless of the initial amount of MFC as the strength of the network is also increased by the presence droplets from the less volatile oil. The density of the porous films decreases as the oil volume fraction increases, which coincides with the larger pore structure observed in these films. Given that $2\pi Rh_f\rho_f$ is the mass of MFC in the dry film with radius R, thickness h_f, and density ρ_f, this mass is equal to the mass of MFC in the emulsion before drying $V_0(1-\varphi_{oil})\,\varphi_{MFC}$. From this relation, we can estimate that at constant concentration of MFC the film density is decreasing with the volume fraction of oil: $\rho_f \sim (1-\varphi_{oil})\,\varphi_{MFC}$. Indeed, Fig. 5a indicates that increase the oil volume fraction to 50 wt% leads to 50 % decrease in the final film density with little change in the film thickness, h_f.

3.4. Effect of the interfacial tension

The capillary force operating in the films is directly related to the surface tension at the air-water interface (Levich & Krylov, 1969). In order to reduce the capillary force which drives the collapse of the

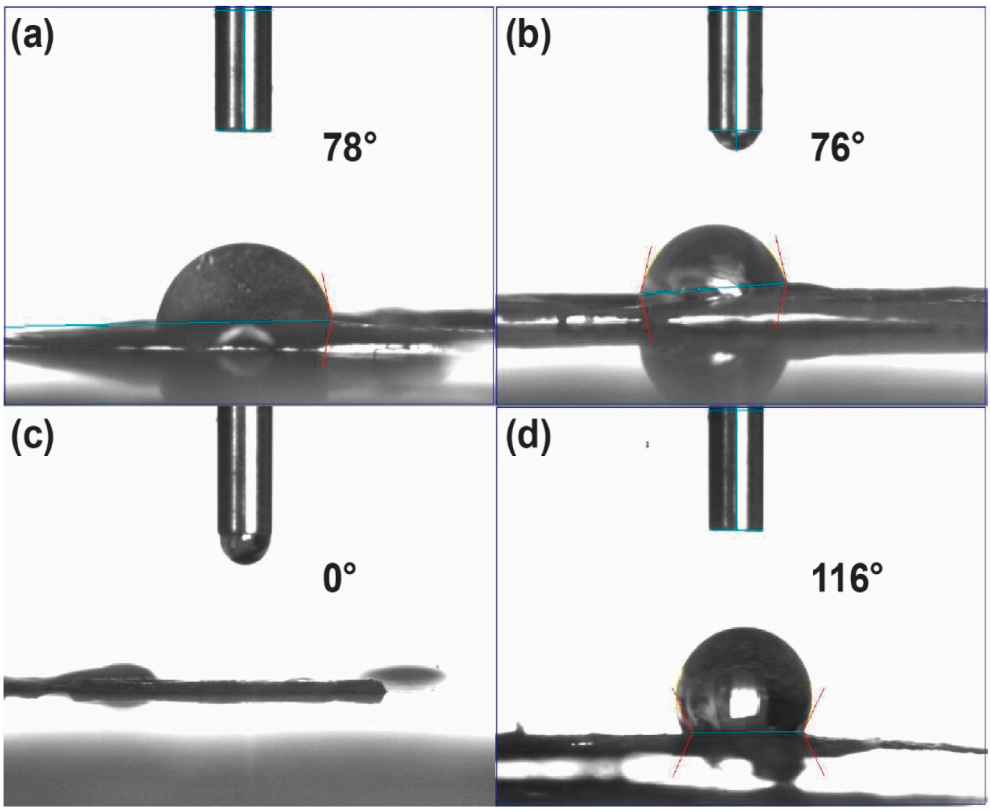

Fig. 9. WCAs of non-silylated and silylated films. (a) non-porous MFC film, (b) silylated non-porous MFC film, (c) porous MFC film prepared from emulsion initially containing 0.3 wt% MFC (7.5 g), 25 wt% decane (2.5 g), and (d) silylated porous MFC film prepared from emulsion initially containing 0.3 wt% MFC (7.5 g), 25 wt% decane (2.5 g).

cellulosic microfibril pores, two typical surfactants, non-ionic (Tween 20) and anionic (SDS), were selected to reduce the surface tension in order to elucidate the effect of capillary force on flattening the structures.

The macroscopic photographic images, optical microscopic images, and in-plane SEM images of the dry films prepared without and with surfactants (i.e., Tween 20 and SDS) are presented in Fig. 6. By adding surfactant, the flattening effect due to capillary force is indeed suppressed and the average pore size is reduced from 480 μm to 190 μm for emulsion containing Tween 20 and to 320 μm for emulsion containing SDS. The size expansion ratio ($r_{pore}/r_{emulsion}$) is reduced from 3.5 to 1.8 for Tween 20 and to 2.5 for SDS. In addition, the film thicknesses measured from lateral SEM images are 30 μm (no surfactant), 270 μm (with Tween 20), and 200 μm (with SDS), respectively, as shown in Fig. 7 (additional data shown in Table S3 of Supporting Information). Thus, the presence of surfactants has a drastic effect on the porosity, as well as structure of the MFC films. Fig. 8 illustrates the dependency of pore size and film thickness on the surface tension of water-air interface. The pore size drops off as surface tension decreases while the film thickness increases instead.

The observed phenomena are possibly a consequence of three surfactant-related effects. First, the surfactant is increasing the emulsion stability by suppressing the coalescence between the droplets, by absorbing on the oil/water interface of the individual droplets, and thus reducing the pore size of the final dry film. Secondly, the surfactants reduce the interfacial tension of water in contact with other phases (e.g., oil, cellulose, and container) and thus weaken the capillary force that drives network to collapse. Lastly, the surfactants function as component of the dry films. The overall consequence is that the thickness of the dry films increases while the pore size is reduced (less flattening effect). Similarly, to the surfactant-free cases, a three-step drying process was observed for emulsions containing surfactants (Fig. S4–S5 in Supporting Information). Using Tween 20 as a surfactant produced highly porous and flexible films, whereas SDS resulted in brittle films. This difference in the film appearance and mechanical properties can be primarily attributed to the structure and integrity of the MFC network. However, the type of surfactant may influence film formation indirectly by affecting emulsion stability, interfacial interactions, and the droplet evolution during drying.

3.5. Silylated porous film

Further modification of the properties of the functional coatings was achieved via silylation. It allowed us to tailor the hydrophobicity on the porous films, thereby increasing water resistance via surface functionalization, improving the film chemical and environmental stability, and tuning interfacial interactions (Rodríguez-Fabià et al., 2022). WCA measurement was performed by placing a droplet of water (~5 μL) on the surface of MFC films to evaluate the wettability of surface. The WCA of the non-porous MFC film was 78° which should be attributed to the smooth surface of the organized cellulose fibrils and presence of minor organic contaminants (Fig. 9a). The lack of porosity does not allow much surface for functionalization and the film displays approximately the same WCA after silylation (Fig. 9b). However, the porous films, with highly heterogeneous surface prepared from emulsion initially containing 0.3 wt% MFC and 25 wt% decane, thereby having plenty of hydroxyl groups and very large exposed surface area, display WCA of 0° (Fig. 9c). The large surface area and the nonplanar rough surface of the porous film much enhanced opportunities for effective silylation. Thus, as shown in Fig. 9d, the WCA is significantly increased from 0 to 116° after the silylation. For completeness, porous MFC films with low amount of oil, 5 wt% decane, and surfactant, 0.16 wt% aqueous Tween 20, were also silylated and analysed (Fig. S6 in Supporting Information). Similarly to Fig. 9c, the nontreated porous film shows high

hydrophilicity with WCA equal to 0°. However, the WCA values significantly increase, up to 70–75°, after silylation. This also indicates that the porous films display more surface hydroxyl groups which provide hydrophilicity and are accessible for the modification. In Table S4 of Supporting Information, the silylation performance based on WCA of the present MFC films are compared to other classes of silylated MFC. The films listed in Table S4 are silylated with diverse silanes under optimized conditions, and comparison focuses on WCA. MFC itself displays very hydrophilic with WCAs ranging from 0 to 40°. Then, after diverse silylation, WCAs are markedly increased to 70∼152°. The porous MFC-decane also possesses very high hydrophilicity with WCA of 0°, and silylation brings out the hydrophobicity up to WCA of 116° which indicates that the silylation technique and the silylated MFC in this study are quite comparable with other studies.

4. Conclusions

This work demonstrates how the use of selected oil droplet templates yields a variety of hierarchal porous MFC thin films. The method for making of these films is simple, efficient, and environmentally friendly. The generation of micropores embedded in fine MFC network is achieved by using oil droplet templates with tunable volatility. The mechanism of formation is elucidated by a proposed three-step mechanism considering coarsening of droplets, capillary force, and vapor pressure based on the observation droplet and pore sizes. Further, pore structure and thickness of oil-templated porous films are tunable by precursor compositions, such as oil fraction and adding surfactant. Finally, the hydrophobicity of the resulting MFC-based porous thin films can be modified to the best match of their areas of application. As an example of such functionalization, hydrophobic methylsilyl groups are successfully attached to the surface of porous MFC, and the hydrophobicity of silylated films is enhanced greatly. The results on oil-templated MFC films lead to better understanding of the new mechanism of pore generation via emulsion templating, resulting in tunable pore structure and thickness.

The goals of this report are to reveal the principles involved in emulsion templating of sustainable coatings; however, the method and the resulting materials could find applications in a broad range of functional and sustainable thin films and coatings. The highly porous cellulose films can provide thermal insulation and mechanical protection in packaging and structural materials. The ability to design biocompatible dual porous cellulosic templates could speed up the developments of cellulose-based tissue scaffolds engineering. The hydrophobized porous films can find applications in novel water-repellent and self-cleaning coatings and surfaces. In order to ensure complete environmental safety and biodegradability, the silanization agents in the future can be replaced with organic hydrophobizing compounds such as alkyl ketene dimers or natural fatty acids. Thus, the principles used in the making of these coatings can expand the outlook of methods aimed at making porous cellulosic materials for future circular technologies.

CRediT authorship contribution statement

Hyung-Ju Kim: Writing – review & editing, Writing – original draft, Visualization, Investigation. **Yan Zeng:** Investigation. **Krassimir P. Velikov:** Writing – review & editing, Funding acquisition, Conceptualization. **Orlin D. Velev:** Writing – review & editing, Supervision, Resources, Funding acquisition, Conceptualization.

Declaration of competing interest

The authors declare that they have no known competing financial interests or personal relationships that could have appeared to influence the work reported in this paper.

Acknowledgment

This work was supported by NanoNextNL and the European Union's Horizon 2020 research and innovation programme under the Marie Skłodowska-Curie grant agreement No 956248. ODV acknowledges support from US NSF grants CMMI-2233399 and DMR-2303581. HJK acknowledges support by the Institute of Civil Military Technology cooperation funded by the Defense Acquisition Program Administration and Ministry of Trade, Industry and Energy of Korea government under grant No. 22-CM-BR-14.

Appendix A. Supplementary data

Supplementary data to this article can be found online at https://doi.org/10.1016/j.foodhyd.2025.111854.

Data availability

Data will be made available on request.

References

Ahmad, M., Kim, B., & Velev, O. D. (2025). Sustainable biopolymer colloids: Advances in morphology for enhanced functionalities. *Langmuir, 41*(11), 7160–7173. https://doi.org/10.1021/acs.langmuir.5c00013

Andresen, M., Johansson, L. S., Tanem, B. S., & Stenius, P. (2006). Properties and characterization of hydrophobized microfibrillated cellulose. *Cellulose, 13*(6), 665–677. https://doi.org/10.1007/s10570-006-9072-1

Aulin, C., Gällstedt, M., & Lindström, T. (2010). Oxygen and oil barrier properties of microfibrillated cellulose films and coatings. *Cellulose, 17*(3), 559–574. https://doi.org/10.1007/s10570-009-9393-y

Baxter, R. I., Rawlings, R. D., Iwashita, N., & Sawada, Y. (2000). Effect of chemical vapor infiltration on erosion and thermal properties of porous carbon/carbon composite thermal insulation. *Carbon, 38*(3), 441–449. https://doi.org/10.1016/S0008-6223(99)00125-6

Beauvais, L. G., Shores, M. P., & Long, J. R. (2000). Cyano-bridged Re6Q8 (Q = S, Se) cluster-cobalt(II) framework materials: Versatile solid chemical sensors. *Journal of the American Chemical Society, 122*(12), 2763–2772. https://doi.org/10.1021/ja994186h

Bennett, M. V., Shores, M. P., Beauvais, L. G., & Long, J. R. (2000). Expansion of the porous solid Na2Zn3[Fe(CN)6]2·9H2O: Enhanced ion-exchange capacity in Na2Zn3[Re6Se8(CN)6]2·24H2O. *Journal of the American Chemical Society, 122*(28), 6664–6668. https://doi.org/10.1021/ja000593d

Binks, B. P., & Horozov, T. S. (2005). Aqueous foams stabilized solely by silica nanoparticles. *Angewandte Chemie International Edition, 44*(24), 3722–3725. https://doi.org/10.1002/anie.200462470

Chaikittisilp, W., Didas, S. A., Kim, H. J., & Jones, C. W. (2013). Vapor-phase transport as a novel route to hyperbranched polyamine-oxide hybrid materials. *Chemistry of Materials, 25*(4), 613–622. https://doi.org/10.1021/cm303931q

Chaikittisilp, W., Kim, H. J., & Jones, C. W. (2011). Mesoporous alumina-supported amines as potential steam-stable adsorbents for capturing CO2 from simulated flue gas and ambient air. *Energy and Fuels, 25*(11), 5528–5537. https://doi.org/10.1021/ef201224v

Dapčević Hadnađev, T., Dokić, P., Krstonošić, V., & Hadnađev, M. (2013). Influence of oil phase concentration on droplet size distribution and stability of oil-in-water emulsions. *European Journal of Lipid Science and Technology, 115*(3), 313–321. https://doi.org/10.1002/ejlt.201100321

Dekker, R. I., Deblais, A., Velikov, K. P., Veenstra, P., Colin, A., Kellay, H., Kegel, W. K., & Bonn, D. (2020). Emulsion destabilization by squeeze flow. *Langmuir, 36*(27), 7795–7800. https://doi.org/10.1021/acs.langmuir.0c00759

Dickinson, E., Ettelaie, R., Kostakis, T., & Murray, B. S. (2004). Factors controlling the formation and stability of air bubbles stabilized by partially hydrophobic silica nanoparticles. *Langmuir, 20*, 8517–8525. https://doi.org/10.1021/la048913k

Drozdov, A. D., & de Claville Christiansen, J. (2020). The effect of porosity on elastic moduli of polymer foams. *Journal of Applied Polymer Science, 137*(10), Article 48449. https://doi.org/10.1002/app.48449

Ferreira, F. V., Souza, A. G., Ajdary, R., de Souza, L. P., Lopes, J. H., Correa, D. S., Siqueira, G., Barud, H. S., Rosa, D., dos, S., Mattoso, L. H. C., & Rojas, O. J. (2023). Nanocellulose-based porous materials: Regulation and pathway to commercialization in regenerative medicine. *Bioactive Materials, 29*, 151–176. https://doi.org/10.1016/j.bioactmat.2023.06.020

Gelb, L. D., Gubbins, K. E., Radhakrishnan, R., & Sliwinska-Bartkowiak, M. (1999). Phase separation in confined systems. *Reports on Progress in Physics, 62*(12), 1573. https://doi.org/10.1088/0034-4885/62/12/201

Hamer, G., & Al-Awadhi, N. (2000). Biotechnological applications in the oil industry. *Acta Biotechnologica, 20*(3–4), 335–350. https://doi.org/10.1002/abio.370200314

Han, J., Xu, H., Zhao, B., Sun, R., Chen, G., Wu, T., Zhong, G., Gao, Y., Zhang, S. L., Yamauchi, Y., Guan, B., Chen, G., Han, J., Sun, R., Zhao, B., Zhong, G., Yamauchi, Y., & Guan, B. (2024). "Hard" emulsion-induced interface super-assembly: A general

strategy for two-dimensional hierarchically porous metal–organic framework nanoarchitectures. *Journal of the American Chemical Society, 146*(28), 18979–18988. https://doi.org/10.1021/jacs.4c02321

Higashiwada, T., Asaoka, H., Hayashi, H., & Kishimoto, A. (2007). Effect of additives on the pore evolution of zirconia based ceramic foams after sintering. *Journal of the European Ceramic Society, 27*(5), 2217–2222. https://doi.org/10.1016/j.jeurceramsoc.2006.08.008

Hollister, S. J. (2005). Porous scaffold design for tissue engineering. *Nature Materials, 4*(7), 518–524. https://doi.org/10.1038/nmat1421

Imhof, A., & Pine, D. J. (1997). Ordered macroporous materials by emulsion templating. *Nature, 389*(6654), 948–951. https://doi.org/10.1038/40105

Jang, K.-S., Kim, H.-J., Johnson, J. R., Kim, W.-G., Koros, W. J., Jones, C. W., & Nair, S. (2011). Modified mesoporous silica gas separation membranes on polymeric hollow fibers. *Chemistry of Materials, 23*, 3025–3028. https://doi.org/10.1021/cm200939d

Juettner, T., Moertel, H., Svinka, V., & Svinka, R. (2007). Structure of kaoline-alumina based foam ceramics for high temperature applications. *Journal of the European Ceramic Society, 27*(2–3), 1435–1441. https://doi.org/10.1016/j.jeurceramsoc.2006.04.029

Kim, H. J., Brunelli, N. A., Brown, A. J., Jang, K. S., Kim, W. G., Rashidi, F., Johnson, J. R., Koros, W. J., Jones, C. W., & Nair, S. (2014). Silylated mesoporous silica membranes on polymeric hollow fiber supports: Synthesis and permeation properties. *ACS Applied Materials and Interfaces, 6*(20), 17877–17886. https://doi.org/10.1021/am504581j

Kim, H. J., Chaikittisilp, W., Jang, K. S., Didas, S. A., Johnson, J. R., Koros, W. J., Nair, S., & Jones, C. W. (2015). Aziridine-functionalized mesoporous silica membranes on polymeric hollow fibers: Synthesis and single-component CO2 and N2 permeation properties. *Industrial & Engineering Chemistry Research, 54*(16), 4407–4413. https://doi.org/10.1021/ie503781u

Kim, H. J., Jang, K. S., Galebach, P., Gilbert, C., Tompsett, G., Conner, W. C., Jones, C. W., & Nair, S. (2013). Seeded growth, silylation, and organic/water separation properties of MCM-48 membranes. *Journal of Membrane Science, 427*, 293–302. https://doi.org/10.1016/j.memsci.2012.10.012

Kishimoto, A., Obata, M., Asaoka, H., & Hayashi, H. (2007). Fabrication of alumina-based ceramic foams utilizing superplasticity. *Journal of the European Ceramic Society, 27*(1), 41–45. https://doi.org/10.1016/j.jeurceramsoc.2006.03.002

Krajnc, P., Stefanec, D., Brown, J. F., & Cameron, N. R. (2005). Aryl acrylate based high-internal-phase emulsions as precursors for reactive monolithic polymer supports. *Journal of Polymer Science, Part A: Polymer Chemistry, 43*(2), 296–303. https://doi.org/10.1002/pola.20501

Lam, S., Velikov, K. P., & Velev, O. D. (2014). Pickering stabilization of foams and emulsions with particles of biological origin. *Current Opinion in Colloid & Interface Science, 19*(5), 490–500. https://doi.org/10.1016/j.cocis.2014.07.003

Lee, M., Wu, B. M., & Dunn, J. C. Y. (2008). Effect of scaffold architecture and pore size on smooth muscle cell growth. *Journal of Biomedical Materials Research - Part A, 87*(4), 1010–1016. https://doi.org/10.1002/jbm.a.31816

Levich, V. G., & Krylov, V. S. (1969). Surface-tension-driven phenomena. *Annual Review of Fluid Mechanics, 1*(1), 293–316. https://doi.org/10.1146/annurev.fl.01.010169.001453, 1969.

Li, J. R., Kuppler, R. J., & Zhou, H. C. (2009). Selective gas adsorption and separation in metal-organic frameworks. *Chemical Society Reviews, 38*(5), 1477–1504. https://doi.org/10.1039/b802426j

Li, W. Y., Xu, L. N., & Chen, J. (2005). Co3O4 nanomaterials in lithium-ion batteries and gas sensors. *Advanced Functional Materials, 15*(5), 851–857. https://doi.org/10.1002/adfm.200400429

Mackay, D., & Van Wesenbeeck, I. (2014). Correlation of chemical evaporation rate with vapor pressure. *Environmental Science and Technology, 48*(17), 10259–10263. https://doi.org/10.1021/es5029074

Mehnert, C. P., Weaver, D. W., & Ying, J. Y. (1998). Heterogeneous heck catalysis with palladium-grafted molecular sieves. *Journal of the American Chemical Society, 120*(47), 12289–12296. https://doi.org/10.1021/ja971637u

Minakuchi, H., Nakanishi, K., Soga, N., Ishizuka, N., & Tanaka, N. (1996). Octadecylsilylated porous silica rods as separation media for reversed-phase liquid chromatography. *Analytical Chemistry, 68*(19), 3498–3501. https://doi.org/10.1021/ac960281m

Mohan, S., Jose, J., Kuijk, A., Veen, S. J., Van Blaaderen, A., & Velikov, K. P. (2017). Revealing and quantifying the three-dimensional Nano- and microscale structures in self-assembled cellulose microfibrils in dispersions. *ACS Omega, 2*(8), 5019–5024. https://doi.org/10.1021/acsomega.7b00536

Murphy, C. M., & O'Brien, F. J. (2010). Understanding the effect of mean pore size on cell activity in collagen-glycosaminoglycan scaffolds. *Cell Adhesion & Migration, 4*, 377–381. https://doi.org/10.4161/cam.4.3.11747

Mysels, K. J. (1986). Surface tension of solutions of pure sodium dodecyl sulfate. *Langmuir, 2*(4), 423–428. https://doi.org/10.1021/la00070a008

Naseri, N., Poirier, J.-M., Girandon, L., Fröhlich, M., Oksman, K., & Mathew, A. P. (2016). 3-Dimensional porous nanocomposite scaffolds based on cellulose nanofibers for cartilage tissue engineering: Tailoring of porosity and mechanical performance. *RSC Advances, 6*, 5999–6007. https://doi.org/10.1039/C5RA27246G

Niño, M. R. R., & Patino, J. M. R. (1998). Surface tension of bovine serum albumin and tween 20 at the air-aqueous interface. *Journal of the American Oil Chemists' Society, 75*(10), 1241–1248. https://doi.org/10.1007/s11746-998-0169-6

Nouar, F., Eckert, J., Eubank, J. F., Forster, P., & Eddaoudi, M. (2009). Zeolite-like metal-organic frameworks (ZMOFs) as hydrogen storage platform: Lithium and magnesium ion-exchange and H-(rho-ZMOF) interaction studies. *Journal of the American Chemical Society, 131*(8), 2864–2870. https://doi.org/10.1021/ja807229a

Pandey, A. (2021). Pharmaceutical and biomedical applications of cellulose nanofibers: A review. *Environmental Chemistry Letters, 19*(3), 2043–2055. https://doi.org/10.1007/s10311-021-01182-2

Pircher, N., Fischhuber, D., Carbajal, L., Strauß, C., Nedelec, J. M., Kasper, C., Rosenau, T., & Liebner, F. (2015). Preparation and reinforcement of dual-porous biocompatible cellulose scaffolds for tissue engineering. *Macromolecular Materials and Engineering, 300*(9), 911–924. https://doi.org/10.1002/mame.201500048

Plackett, D., Anturi, H., Hedenqvist, M., Ankerfors, M., Gällstedt, M., Lindström, T., & Siró, I. (2010). Physical properties and morphology of films prepared from microfibrillated cellulose and microfibrillated cellulose in combination with amylopectin. *Journal of Applied Polymer Science, 117*(6), 3601–3609. https://doi.org/10.1002/app.32254

Proust, A., Thouvenot, R., & Gouzerh, P. (2008). Functionalization of polyoxometalates: Towards advanced applications in catalysis and materials science. *Chemical Communications, 16*, 1837–1852. https://doi.org/10.1039/b715502f

Rodríguez-Fabià, S., Torstensen, J., Johansson, L., & Syverud, K. (2022). Hydrophobization of lignocellulosic materials part II: Chemical modification. *Cellulose, 29*(17), 8957–8995. https://doi.org/10.1007/s10570-022-04824-y

Seo, J. S., Whang, D., Lee, H., Jun, S. I., Oh, J., Jeon, Y. J., & Kim, K. (2000). A homochiral metal-organic porous material for enantioselective separation and catalysis. *Nature, 404*(6781), 982–986. https://doi.org/10.1038/35010088

Sherbo, R. S., Moreno-Gonzalez, M., Johnson, N. J. J., Dvorak, D. J., Fork, D. K., & Berlinguette, C. P. (2018). Accurate coulometric quantification of hydrogen absorption in palladium nanoparticles and thin films. *Chemistry of Materials, 30*(12), 3963–3970. https://doi.org/10.1021/acs.chemmater.8b01324

Sherif, F. G., & Shyu, L.-J. (1991). Emulsion precipitation of Yttria-Stabilized Zirconia for Plasma spray coatings. *Journal of the American Ceramic Society, 74*(2), 375–380. https://doi.org/10.1111/j.1151-2916.1991.tb06890.x

Siró, I., & Plackett, D. (2010). Microfibrillated cellulose and new nanocomposite materials: A review. *Cellulose, 17*(3), 459–494. https://doi.org/10.1007/s10570-010-9405-y

Stull, D. R. (1947). Vapor pressure of pure substances. Organic and inorganic compounds. *Industrial and Engineering Chemistry, 39*, 517–540. https://doi.org/10.1021/ie50448a022

Sun, Y., Chu, Y., Wu, W., & Xiao, H. (2021). Nanocellulose-based lightweight porous materials: A review. *Carbohydrate Polymers, 255*, Article 117489. https://doi.org/10.1016/j.carbpol.2020.117489

Tokuyama, H., & Kanehara, A. (2007). Novel synthesis of macroporous poly(N-isopropylacrylamide) hydrogels using oil-in-water emulsions. *Langmuir, 23*(22), 11246–11251. https://doi.org/10.1021/la701492u

Wege, H. A., Kim, S., Paunov, V. N., Zhong, Q., & Velev, O. D. (2008). Long-term stabilization of foams and emulsions with in-situ formed microparticles from hydrophobic cellulose. *Langmuir, 24*(17), 9245–9253. https://doi.org/10.1021/la801634j

Wexler, A. (1976). Vapor pressure formulation for water in range 0 to 100 C. A revision. *Journal of Research of the National Bureau of Standards Section A: Physics and Chemistry, 80A*(5 and 6), 775. https://doi.org/10.6028/jres.080a.071

Wu, T., Chen, G., Han, J., Sun, R., Zhao, B., Zhong, G., Yamauchi, Y., & Guan, B. (2023). Construction of three-dimensional dendritic hierarchically porous metal–organic framework nanoarchitectures via noncentrosymmetric pore–induced anisotropic assembly. *Journal of the American Chemical Society, 145*(30), 16498–16507. https://doi.org/10.1021/jacs.3c03029

Wu, C., Yin, P., Zhu, X., OuYang, C., & Xie, Y. (2006). Synthesis of hematite (α-Fe2O3) nanorods: Diameter-size and shape effects on their applications in magnetism, lithium ion battery, and gas sensors. *Journal of Physical Chemistry B, 110*(36), 17806–17812. https://doi.org/10.1021/jp0633906

Yang, J., Chen, X., Tantai, S., Lv, Y., Zhao, L., Fu, S., & Tang, C. (2025). Pore formation mechanism and size regulation study of atmospheric dried cellulose nanofiber aerogel templated by emulsions. *International Journal of Biological Macromolecules, 299*, Article 140214. https://doi.org/10.1016/j.ijbiomac.2025.140214

Yuan, Z. Y., & Su, B. L. (2006). Insights into hierarchically meso-macroporous structured materials. *Journal of Materials Chemistry, 16*(7), 663–677. https://doi.org/10.1039/b512304f